iScience

CellPress
OPEN ACCESS

Article

Pushing the Envelope in Battery Estimation Algorithms

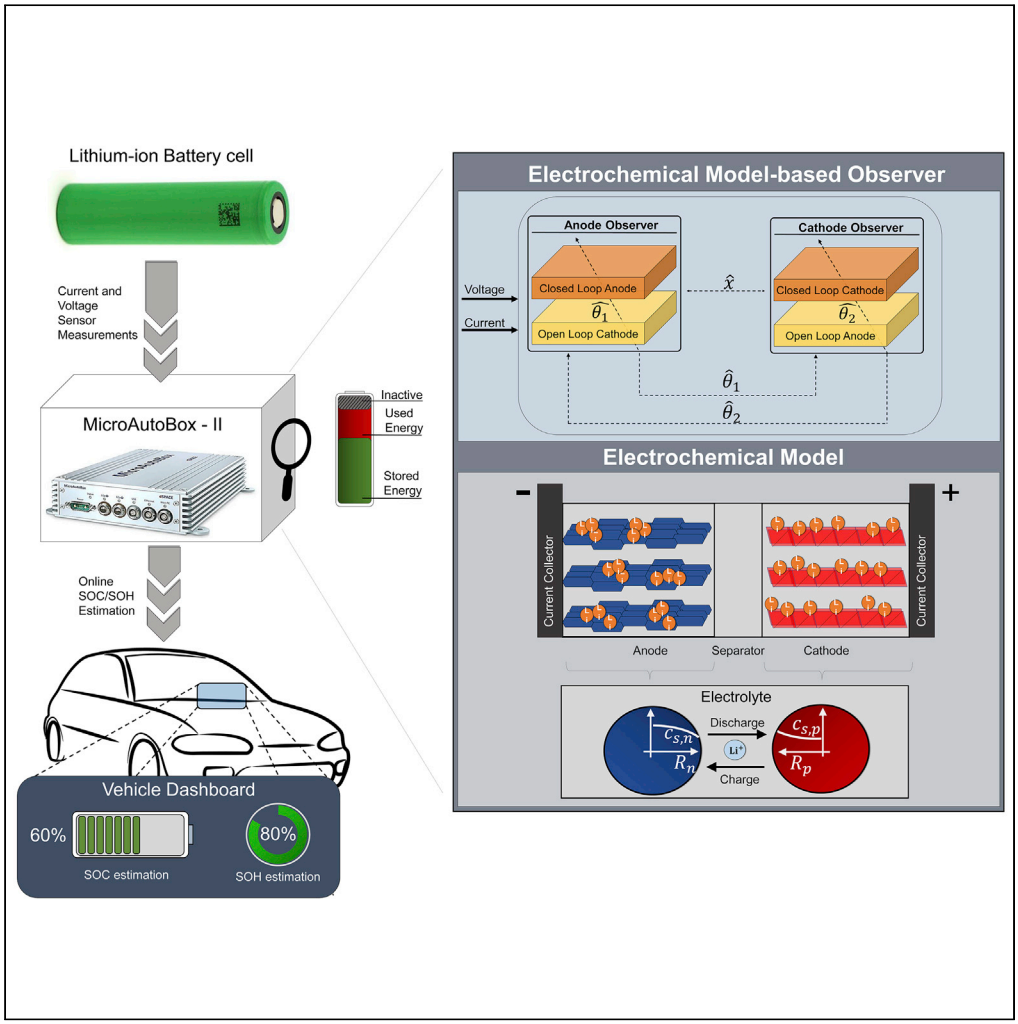

Anirudh Allam, Edoardo Catenaro, Simona Onori

sonori@stanford.edu

HIGHLIGHTS

An electrochemical adaptive interconnected observer is used to estimate cell SOC/SOH.

A description for setting up state-of-the-art BIL experiments is presented.

A SOC/SOH estimation error of 2% with respect to the measured true values is reported.

The observer is robust to noise, quantization errors, and initialization errors.

Allam et al., iScience 23, 101847
December 18, 2020
https://doi.org/10.1016/j.isci.2020.101847

iScience

CellPress
OPEN ACCESS

Article

Pushing the Envelope in Battery Estimation Algorithms

Anirudh Allam,[1] Edoardo Catenaro,[1] and Simona Onori[1,2,*]

SUMMARY

Accurate estimation of lithium-ion battery health will (a) improve the performance and lifespan of battery packs in electric vehicles, spurring higher adoption rates, (b) determine the actual extent of battery degradation during usage, enabling a health-conscious control, and (c) assess the available battery life upon retiring of the vehicle to re-purpose the batteries for "second-use" applications. In this paper, the real-time validation of an advanced battery health estimation algorithm is demonstrated via electrochemistry, control theory, and battery-in-the-loop (BIL) experiments. The algorithm is an adaptive interconnected sliding mode observer, based on a battery electrochemical model, which simultaneously estimates the critical variables such as the state of charge (SOC) and state of health (SOH). The BIL experimental results demonstrate that the SOC/SOH estimates from the observer converge to an error of 2% with respect to their true values, in the face of incorrect initialization and sensor signal corruption.

INTRODUCTION

The expanding global electric vehicle market is an indication of a conscious effort by civilization to reduce the reliance on fossil fuels and steadily replace it with a more environment-friendly energy storage and conversion system. Lithium-ion batteries (LIBs) are electrochemical energy storage systems that have found themselves to be the preferred choice for the electrification of the transportation sector and being considered as a storage solution in the renewable energy sector owing to their superior specific energy and power density. Despite these benefits, LIBs are known to be susceptible to abuse (such as thermal runaway (Wang et al., 2012)) due to complex degradation mechanisms, which may lead to safety and reliability issues. For this reason, an LIB system is accompanied with a battery management system (BMS) with the main objective of ensuring its safety, performance, and reliability. The Battery Management System (BMS) is tasked with the responsibility of monitoring the critical battery internal variables that represent the current state of charge (SOC) and state of health (SOH) (Rahimi-Eichi et al., 2013) and uses that information for maintaining conditions conducive for a longer battery lifespan. Typically, these critical variables are not available for measurement via sensors, and hence, the BMS has to "estimate" these variables from available battery current, voltage, and temperature data.

Motivation

Model-based observers are widely researched in the literature for the combined estimation of SOC and SOH. These model-based estimation algorithms can be broadly classified into two main groups, based on the type of battery model they use: equivalent circuit model and electrochemical model. While the estimation algorithms based on equivalent circuit models (Chen et al., 2014; Kim, 2006) are computationally inexpensive and easy to implement, it needs to be pointed out that they do no offer physical insight into battery's internal dynamics, and a large amount of experimental effort goes into accurately calibrating these lumped-parameter models for different operating conditions. On the other hand, electrochemical models are characterized by lithium ion transport mechanisms, and hence, using such detailed physics-based models for estimation lends itself well to accurately monitoring the internal battery variables such as lithium concentration (Dey et al., 2015; Moura et al., 2017; Allam and Onori, 2018, 2020b) and by extension the SOC and SOH. Naturally, electrochemical model-based estimation is more powerful and can also provide key physical insights to the BMS to take precise control decisions to improve safety and lifespan. However, the bottleneck with this method is that it is computationally expensive since the model is described by a system of partial differential equations (PDEs).

[1]Department of Energy Resources Engineering, Stanford University, Stanford, CA 94305, USA

[2]Lead Contact

*Correspondence: sonori@stanford.edu

https://doi.org/10.1016/j.isci.2020.101847

Consequently, discussions on the real-time performance of these electrochemical model-based observers have been lacking in the literature. Further, there is no documented evidence of this method being implemented on real hardware. Therefore, one of the key steps in demonstrating the strength of the class of electrochemical model-based observers is to show that they can be robust against challenges introduced during real-time implementation, such as noisy signals and computational constraints. Hence, it is imperative to test such an observer in real time on a physical hardware to gauge its performance holistically.

To that end, this work aims to present a detailed experimental framework to enable the real-time validation of a reduced-order electrochemical model-based observer via battery-in-the-loop (BIL) experiments by using state-of-the-art equipment.

Battery-in-the-Loop Experiments

Modern day electric vehicles are complex systems consisting of numerous electronic control units (ECUs), such as the BMS ECU, that have specific functionalities, and they also interact with each other. Each ECU may have high development cost and time associated with it. The primary objective of automotive manufacturers is to reduce development and testing time of ECUs, testing costs, and ensure safety while fault testing and validating these subsystems. For that reason, the ECU development workflow involves different simulation/testing stages such as

1. Model-in-the-loop (MIL): The MIL test is conducted at the initial stages of the V-model workflow, wherein the plant model to be controlled and the controller (ECU) model are in a simulation environment, and no physical hardware components are involved.
2. Software-in-the-loop (SIL): The SIL stage involves the code generation of the controller (ECU) model, which is tested with the plant model in a simulation environment with no physical hardware components.
3. Hardware-in-the-loop (HIL): The HIL stage involves code generation of both, the plant and controller models. The plant code is downloaded to a real physical hardware simulator and the controller code is hosted on an embedded controller. Physical hardware components and connections such as sensors, actuators, physical wiring interconnections are a part of this test.

Each of the above tests is conducted at different stages of the ECU development workflow to gain confidence in the performance of the controller algorithm, both in simulation and hardware environment.

In the above described HIL setup, if the hardware simulating the plant dynamics is replaced with a real physical system, which in the context of this paper is a lithium-ion battery, then it is referred to as the BIL test. It follows that the code hosted on the embedded controller is that of the estimation algorithm. BIL is a more powerful validation approach than the HIL, wherein the developed estimation algorithm can be tested in real time over the actual battery cell rather than its model. This test results in reduced development time and cost as it allows the algorithm to be tested on hardware in the early stages of development. Further, this test enables an iterative process of improving and correcting the algorithm without having to spend time waiting for the HIL test stage. The main components of a BIL, as shown in Figure 1, are as follows:

1. a lithium-ion battery,
2. a programmable direct current (DC) load to charge/discharge the battery according to a predetermined input current cycle,
3. an embedded controller that hosts the estimation algorithm, and
4. a controller area network (CAN) bus to transmit the measured current, voltage, and temperature data from the DC load to the controller. In this work, the lithium-ion battery is a cylindrical 2Ah cell with a positive electrode of nickel managanese cobalt (NMC) oxide and a negative electrode of graphite. The programmable DC Load is an Arbin LBT21024 for cycling battery systems, and the embedded controller is a dSPACE MicroAutoBox-II.

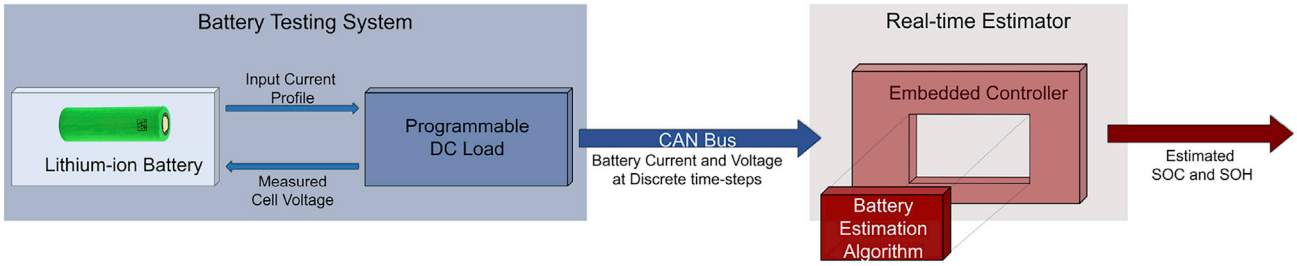

Figure 1. BIL Scheme
General schematic of a battery-in-the-loop (BIL) setup.

Related Literature and Contributions

In the battery modeling and estimation literature, HIL and BIL testing has been limited to the use of battery equivalent circuit models (Song et al., 2013; Kim et al., 2014a, 2014b; Zhang et al., 2018; Tara et al., 2013) and estimation algorithms ranging from unscented Kalman filters (He et al., 2016), adaptive H-infinity filters (Zhang et al., 2016), dual H-infinity filters (Chen et al., 2017) to adaptive extended Kalman filters (Zhang et al., 2017). BIL experiments have been used, wherein a real physical battery system is connected to a controller, to evaluate energy management strategy algorithms for plug-in hybrid and hybrid electric vehicles (Kim et al., 2014a, 2014b; Zhang et al., 2018; Tara et al., 2013). Battery equivalent circuit models hosted in an HIL platform are used for testing commercial BMS controllers (Barreras et al., 2016; Dai et al., 2013). Moreover, for the validation of battery state estimation algorithms, a HIL experimental platform has been used to estimate SOC (He et al., 2010, 2016; Zhang et al., 2016, 2017; Chen et al., 2017), capacity (SOH) (Chen et al., 2017), and state of energy (Zhang et al., 2016). The embedded controllers used in the literature range from dSPACE simulators/Autobox (Song et al., 2013) (Barreras et al., 2016), real time operating system (RTOS) µCOS-II platform (He et al., 2016), and xPC Target (Zhang et al., 2016) (Zhang et al., 2017). It is to be noted that every implementation of a battery model in the HIL and BIL platforms found in the open literature is based on a battery equivalent circuit model. However, with the need for advanced BMS designs in the future, it is prudent to harness the strengths of rich physics-based modeling and control theory tools by exploring the implementation of battery electrochemical models and other types of model-based observers. To that end, the key contributions of the proposed work are as follows:

1. implementing a real-time validation approach for an electrochemical model-based adaptive interconnected observer for the combined estimation of SOC and SOH (Allam and Onori, 2020a, 2020b) showing that it is computationally feasible,
2. describing the steps to be undertaken to establish a BIL experimental setup with state-of-the-art equipment, and
3. demonstrating the real-time performance of the estimation algorithm in terms of robustness, under noisy input signals and over different drive cycles.

RESULTS AND DISCUSSION

Electrochemical Model

The lithium-ion battery electrochemical model is characterized by a system of partial differential algebraic equations describing the transport of lithium in the solid and electrolyte phase via mass and charge conservation laws (Doyle et al., 1993). This model, popularly known as the pseudo-two-dimensional (P2D) model, is a high-dimensional and high-fidelity electrochemical model, which was traditionally used for battery design and modeling purposes. However, in this work, a low-fidelity reduced-order electrochemical model derived from the P2D model, referred to as the single particle model (SPM), is used with an aim to lend itself to observer design for online state/parameter estimation and to minimize computational effort, thereby enabling the model to be run on real-time embedded controllers that have limited power capability and resources. The SPM assumes that each electrode can be abstracted by a single spherical particle (Santhanagopalan et al., 2006), as shown in Figure 2A. Further, a uniform current density is assumed in each electrode, and dynamics in the electrolyte phase are neglected. These assumptions ensure that the SPM has a lower computational burden compared to the full-order model (P2D) at the cost of accuracy. In

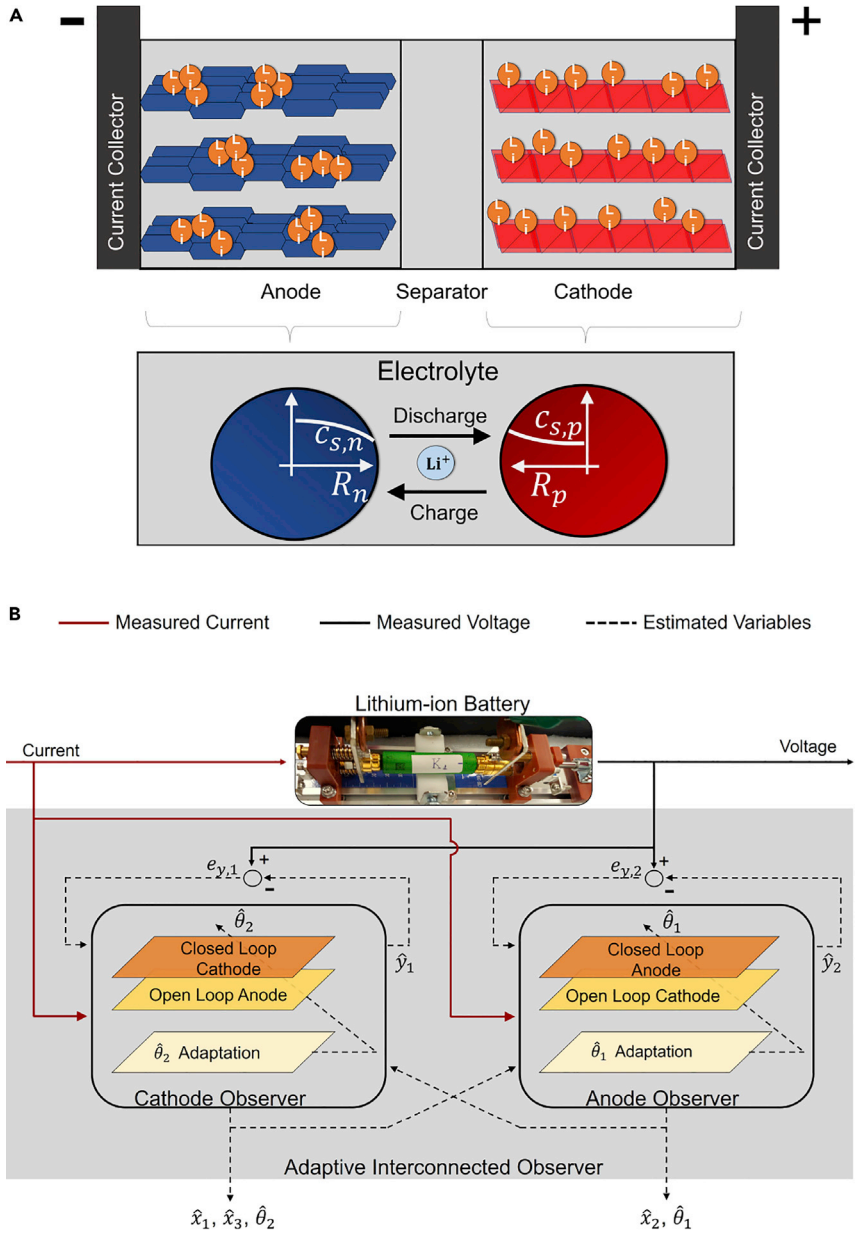

Figure 2. Components of an Electrochemical Model-based Adaptive Interconnected Observer

(A and B) (A) Representation of a lithium-ion cell and the schematic of a single particle model (See Table S1 in the Supplemental Information for values of the SPM parameters), and (B) the interconnected adaptive observer structure for the estimation of lithium concentration states ($\hat{x}_1, \hat{x}_2$), total cell capacity ($\hat{x}_3$), anode diffusion coefficient ($\hat{\theta}_1$), and the SEI layer ionic conductivity ($\hat{\theta}_2$).

particular, due to neglecting the electrolyte dynamics, the model's performance at higher C-rates (wherein C-rate is defined as the rate of current in normalized form, $C-rate = I_{batt}/Q_{nom}$, where I_{batt} is the applied current and Q_{nom} is the nominal battery capacity) is inaccurate.

The SPM predicts the voltage behavior of the battery when the cell is at the beginning of its life. However, as the battery ages, this expression will fail to reproduce the exact degrading behavior of the cell. To that end, this paper aims to incorporate terms that explicitly depend on degradation into the SPM formulation. This work assumes that the solid electrolyte interphase (SEI) layer growth is the major degradation mechanism in lithium-ion batteries. The SEI layer growth is due to the electrolyte solvent reduction at the

interface of the negative electrode and electrolyte, which consumes cyclable lithium ions, thereby reducing the cell capacity and power capability (increased resistance). The relationship between capacity fade and power fade due to SEI layer growth is exploited to derive terms that can be incorporated into the SPM. Therefore, the voltage predicted by the newly formulated aging-enhanced SPM will replicate the waning performance of the battery as it ages.

For the real-time implementation of the SPM, the PDEs describing the transport of lithium in the solid phase are spatially discretized using the finite difference method to obtain a system of ordinary differential equations (ODEs) for both electrodes. Subsequently, the ODEs and the algebraic equations are reformulated into a state-space formulation, which is expounded in the Transparent Methods in the Supplemental Information.

Model-Based Observer

In most physical systems, not all the internal state variables can be directly measured via sensors. In such cases, model-based observers can be employed to use the system inputs and outputs, which are available via sensor measurements, to estimate the non-measurable internal states of a system. This, however, is contingent on the system's observability, wherein observability is a fundamental property of the system that guarantees that the internal states of a system can be inferred based on output sensor measurements. It follows that if a system is observable, then the internal state variables can indeed be reconstructed using the output measurements. Furthermore, state observers can be generally classified into two types: open-loop observer and closed-loop observer. The open-loop observer estimates the internal states, from a given set of initial conditions, by simulating the model without using the actual output sensor measurements. The major issue with this approach is that the error between model output and the measurements is never accounted for, and hence, any incorrect initial conditions will be propagated in time and not be corrected, resulting in state estimates that diverge from the true values. On the other hand, the closed-loop observer measures the error between the model output and sensor measurements and applies a gain proportional to this error to correct the estimated states such that the measurement error is driven to zero. This ensures that despite incorrect initialization of states, the inclusion of this feedback mechanism forces the closed-loop observer to estimate the states accurately over time.

In the context of electrochemical model-based observers for battery state estimation, the internal non-measurable states (such as lithium concentration in cathode and lithium concentration in anode) need to be inferred from the cell output voltage measurements. The weak observability of the battery system while simultaneously trying to estimate the lithium concentration in both electrodes is studied in the literature (Di Domenico et al., 2010; Bartlett et al., 2016), and the different methods to overcome the observability issues and their respective drawbacks are documented (Allam and Onori, 2018). One of the methods reports that the system is observable from the cell voltage measurements under the assumption that the lithium concentration in one electrode is simulated in open-loop fashion while the lithium concentration in the other electrode is estimated in closed-loop fashion (Bartlett et al., 2016). This, of course, assumes that the initial conditions of the open-loop model are perfectly known, which eventually allows the closed-loop estimates to converge to their true values. This approach will not work in realistic scenarios where the initial lithium concentration in both electrodes is unknown, which will result in the state estimates from the single electrode observer to diverge from the true values over time.

The idea of a single electrode observer is extended in this work by introducing dual observers, wherein a single electrode observer is dedicated for each electrode, hereby referred to as a cathode observer and an anode observer. In the cathode observer, the lithium concentration in the cathode is estimated in a closed-loop fashion while the lithium concentration in the anode is estimated in an open-loop fashion. Thus, the output error between the cathode observer's output and the cell voltage measurements is accounted for while estimating the cathode concentration states. Likewise, the structure of the anode observer is similar except that the lithium concentration in the anode is estimated in closed-loop fashion while the lithium concentration in the cathode is estimated in an open-loop fashion. Clearly, the open-loop models of both observers are still susceptible to providing erroneous values under incorrect initial conditions, which will result in faulty closed-loop estimates. This issue is overcome by realizing a bidirectional interconnection between the two observers that can correct the open-loop models over time. The closed-loop estimate of cathode's lithium concentration from the cathode observer is fed to the anode observer to correct the open-loop model of the cathode, whereas the closed-loop estimate of anode's lithium concentration from the anode

observer is fed to the cathode observer to correct the open-loop model of the anode. This bidirectional interconnection ensures that despite incorrect initialization of the concentration states in both electrodes, the open-loop models in both observers are updated and corrected, which ultimately ensures that the closed-loop estimates will converge to their respective true values.

While the interconnected observer described above can concurrently estimate the lithium concentration in the cathode and the anode (Allam and Onori, 2018) to provide information on SOC, it is not equipped to estimate SOH indicators like the cell capacity (SOH). This is because as battery ages, some of the electrochemical model parameters identified at the beginning of life will change due to battery degradation mechanisms. Using such a model for estimation purposes throughout the entire lifespan of the battery will result in state estimates (SOC and SOH) to diverge since the model will no longer remain accurate with aging. Hence, an adaptation mechanism is considered to ensure the aging-sensitive model parameters are adapted as the battery degrades, resulting in an adaptive interconnected observer. This ensures that the combined estimation of the states and parameters remain accurate despite aging.

To that end, an adaptive interconnected observer (Allam and Onori, 2020a, 2020b), as shown in Figure 2B, is developed to concurrently estimate the lithium concentration in both electrodes, cell capacity, and aging-sensitive model parameters, despite any incorrect initialization of states and parameters. An aging-enhanced SPM, introduced earlier, is used as a basis to develop the observer, and the choice of observer structure is a sliding mode observer, which is a class of robust observers that can handle model uncertainties via variable structure gains. The sensor measurements of current and voltage of a lithium-ion cell act as an input to the adaptive interconnected observer. The cathode observer estimates the lithium concentration in the cathode ($\widehat{x}_1$), cell capacity ($\widehat{x}_3$), and the SEI layer ionic conductivity ($\widehat{\theta}_2$). The anode observer estimates the lithium concentration in the anode ($\widehat{x}_2$) and the anode diffusion coefficient ($\widehat{\theta}_1$). Further, the practical stability of the adaptive interconnected observer's estimation error dynamics has been proved analytically (Allam and Onori, 2020b), which ensures that the estimated variables converge around the respective true values within a bounded error ball of radius defined by the uncertainties in the aging-enhanced SPM.

It has to be pointed out that the continuous-time adaptive interconnected observer formulation (Allam and Onori, 2020b) cannot be directly implemented on an embedded controller. Since the sensor measurements in a real system are available at discrete sample times, the continuous-time system needs to be sampled at particular time intervals to obtain a discrete-time system. The discrete-time formulation of the adaptive interconnected observer (reported in the Transparent Methods in the Supplemental Information) can be readily implemented on an embedded controller in real time for BIL experiments.

BIL Experimental Results

Experiments are conducted on a cylindrical lithium-ion cell with graphite at the negative electrode and NMC at the positive electrode. The cell capacity measured using the manufacturer's recommended discharge current of 1C is 1.95Ah. The cell is introduced into the BIL setup as shown and described in the Transparent Methods in the Supplemental Information (See Figures S1 and S2 for experimental setup and connections, Tables S2 and S3 for specification of the cell and equipment). The cell is subjected to dynamic current profiles, such as the Urban Dynamometer Driving Schedule (UDDS) and the world harmonized light-duty vehicles test procedure (WLTP), through MITS PRO software and the Arbin LBT21024 equipment. The Arbin system measures the current and voltage of the battery and transmits them via Arbin's CAN port every 0.1s, which is received by the CAN port of the dSPACE MicroAutoBox-II (see Figures S3–S5, and Table S4 in Transparent Methods in the Supplemental Information for relevant CAN communication specifications). These received signals are fed as an input to the adaptive interconnected observer running in real time hosted by the MicroAutoBox.

To demonstrate the robustness of the observer, the model is incorrectly initialized to verify if it can converge to the true values despite the incorrect initialization and in the presence of sensor noises and corrupted input signals. The estimated variables by the observer, which are the SOC and cell capacity (SOH), are compared with the true SOC value from the battery computed using the coulomb counting method and to the true measured capacity of the battery (1.95Ah), respectively. In addition, the estimated variables from these BIL results are also compared to the MIL test results which are performed via offline simulation with no computational constraints or input signal corruption. This comparison with measured true benchmark values allows the user to evaluate the performance of the real-time effectiveness of an observer.

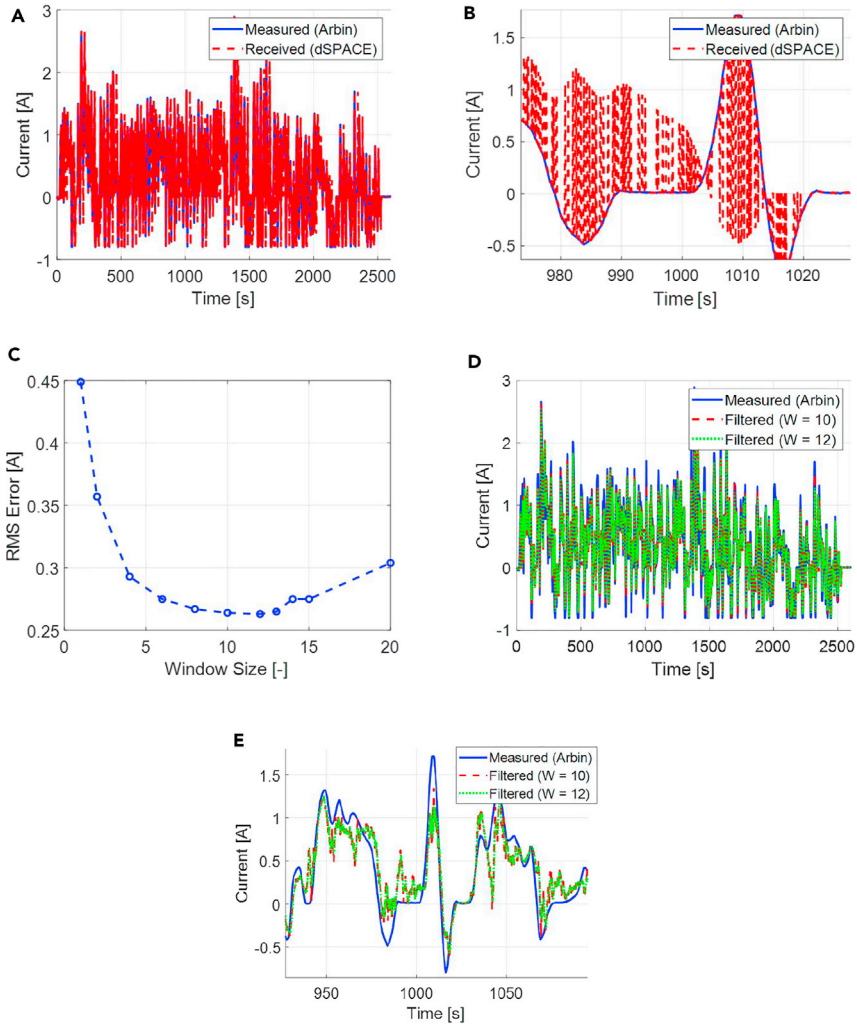

Figure 3. Observer Input Signal Corruption and Correction

(A–E) (A) Signal comparison between measured current by the Arbin and the corrupted signal received at the dSPACE MicroAutoBox via CAN bus, (B) zoomed-in version of the current comparison plot, (C) the RMSE plot for different window sizes for the moving average filter, (D) the comparison of measured current by the Arbin and the filtered signal at the dSPACE MicroAutoBox, and (E) the zoomed-in version of the measured current and filtered current plot.

It is noted that the signals (current, voltage) transmitted over the CAN bus from the Arbin to the dSPACE MicroAutoBox every 0.1s are corrupted with quantization errors. It is understood that due to the fast sampling time of 0.1s, the signal received at the MicroAutoBox is highly corrupted, as shown in Figures 3A and 3B. As a result, a moving average filter is introduced in the MicroAutoBox to smooth out the signals before feeding them as an input to the adaptive observer. The window size of the moving average filter is chosen to be 10. This size is chosen after running the experiments for various window sizes and selecting the one which outputs a filtered signal that is closest to the measured signals (the closeness to the measured signal is verified by computing the RMS error), as shown in Figure 3C. The resulting filtered signal is well constructed and an approximate version of the actual measured current signal, as shown in Figures 3D and 3E, which is then fed to the observer algorithm hosted in the MicroAutoBox.

The results for the UDDS and the WLTP profiles are shown in Figures 4A and 4B, respectively. For both cases, the lithium concentration (SOC) states are initialized with an error of 15%, and the capacity (SOH) state is initialized with an error of 7%. The cell is fully charged before subjecting it to the UDDS profile, whereas the cell is at 80% SOC before applying the WLTP profile. In Figures 4A and 4B, the legend MIL

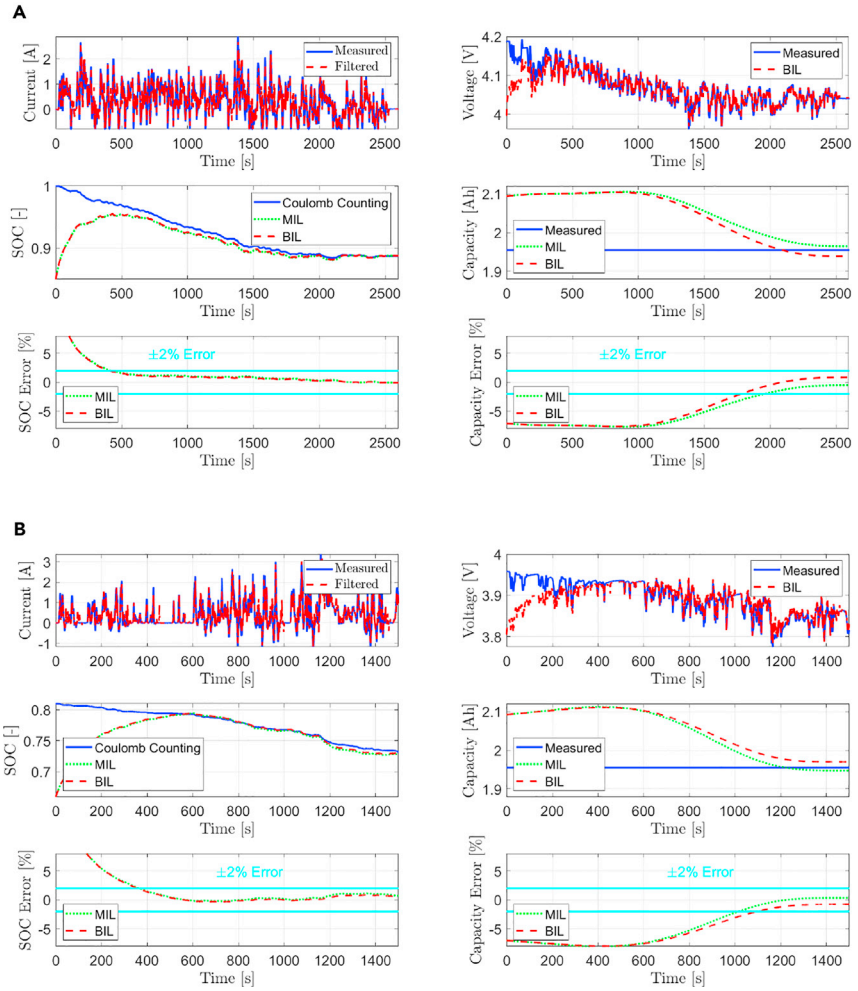

Figure 4. Battery SOC/SOH Estimation Results

(A and B) SOC/SOH estimation results for the (A) UDDS and (B) WLTP input current profiles. The plot shows the input current signal, voltage, SOC and capacity estimation results, and the estimation error plots for SOC and capacity.

refers to the estimated states by the adaptive observer in an offline simulation environment, where the input to the observer is fed from the measured experimental data and not the filtered input signals, whereas BIL refers to the estimates from the real-time validation with the physical battery. Note that the initial SOC estimation error is higher during the initial phase of the experiments because the observer is incorrectly initialized. The cathode concentration state variables (which makes up the bulk SOC) are initialized with an error of 15% at the beginning to verify if the observer can overcome this initial incorrect error and still converge with the true value over time. As observed, the BIL estimation is comparable to the MIL despite corrupted input signals. The results further validate the practical stability notion by showing that the SOC and capacity estimates always stay bounded within the $\pm 2\%$ error with respect to the reference/measured values.

Conclusions

In this work, the importance of real-time validation approaches for battery estimation algorithms is motivated and a description of the BIL experimental setup is presented. The paper focuses on pushing the envelope in battery estimation algorithms by implementing an electrochemical model-based observer in real time, thereby bridging the gap between theory and real-time hardware validation without compromising on the performance. Every component required to setup the BIL experiments is described in detail, and the steps to establish the communication between a physical lithium-ion cell and the embedded controller that hosts the adaptive observer are outlined. The BIL validation of the adaptive observer is performed over two dynamic driving profiles

– UDDS and WLTP. The SOC and SOH estimation results from the BIL are always bounded within ± 2% of their respective true values, despite the corruption of the input signal in real time. The validation demonstrates that an advanced electrochemical model-based estimation algorithm can be run in real time with good accuracy against noises and errors induced due to real physical connections. The use of such algorithms in real-time applications holds the key to improve battery lifespan, enable accurate diagnosis/prognosis, and identify cells of similar health for the feasibility of using them in "second-use" applications upon retirement.

Limitations of the Study

The proposed adaptive interconnected observer estimates the cell capacity (SOH) by exploiting the relationship between power fade and capacity fade due to the growth of the SEI layer at the anode. This observer assumes that SEI layer growth is the primary degradation mechanism plaguing lithium-ion batteries. While this may be true for certain applications, as cells continue to age and based on their usage, they may undergo different degradation mechanisms such as lithium plating. It is worth understanding how effects of other degradation mechanisms can be incorporated into the aging-enhanced SPM to more accurately estimate the cell capacity in the presence of degradation caused due to mechanisms other than SEI layer growth.

Further, the work presented in this paper is for the SOC/SOH estimation of individual cells. Future work will involve extending it to a battery pack that has been aged over multiple cycles, which is composed of multiple lithium-ion cells connected in series and/or parallel, to verify the effectiveness of the observer for large-scale battery packs in real time.

Resource Availability

Lead Contact

Further information and requests should be directed to and will be fulfilled by the Lead Contact, Simona Onori (sonori@stanford.edu).

Materials Availability

This study did not generate new materials.

Data and Code Availability

The data and code supporting the current study is available from the Lead Contact on request.

METHODS

All methods can be found in the accompanying Transparent Methods supplemental file.

SUPPLEMENTAL INFORMATION

Supplemental Information can be found online at https://doi.org/10.1016/j.isci.2020.101847.

ACKNOWLEDGMENTS

N/A.

AUTHOR CONTRIBUTIONS

S.O. conceived the idea. A.A worked on the discrete-time model-based observer. E.C. prepared the experimental setup for the BIL. A.A. and E.C. carried out the experiments. A.A., E.C., and S.O. wrote the manuscript.

DECLARATION OF INTERESTS

A.A. and S.O. have a patent entitled "Battery Monitoring System", (Application No. PCT/US2020/022999, Publication Date: 17 September, 2020) which is related to this work.

Received: July 31, 2020
Revised: September 26, 2020
Accepted: November 17, 2020
Published: December 18, 2020

REFERENCES

Allam, A., and Onori, S. (2018). An interconnected observer for concurrent estimation of bulk and surface concentration in the cathode and anode of a lithium-ion battery. IEEE Trans. Ind. Electron. *65*, 7311–7321.

Allam, A., and Onori, S. (2020a). Battery Monitoring System, App. PCT/US20/22999. https://patents.google.com/patent/WO2020186269A1/en?oq=WO2020186269+-+BATTERY+MONITORING+SYSTEM.

Allam, A., and Onori, S. (2020b). Online capacity estimation for lithium-ion battery cells via an electrochemical model-based adaptive interconnected observer. IEEE Trans. Control Syst. Technol. https://ieeexplore.ieee.org/document/9195005.

Barreras, J.V., Fleischer, C., Christensen, A.E., Swierczynski, M., Schaltz, E., Andreasen, S.J., and Sauer, D.U. (2016). An advanced hil simulation battery model for battery management system testing. IEEE Trans. Industry Appl. *52*, 5086–5099.

Bartlett, A., Marcicki, J., Onori, S., Rizzoni, G., Yang, X., and Miller, T. (2016). Electrochemical model-based state of charge and capacity estimation for a composite electrode lithium-ion battery. IEEE Trans. Cont. Syst. Tech. *24*, 1.

Chen, C., Xiong, R., and Shen, W. (2017). A lithium-ion battery-in-the-loop approach to test and validate multiscale dual h infinity filters for state-of-charge and capacity estimation. IEEE Trans. Power Electron. *33*, 332–342.

Chen, X., Shen, W., Cao, Z., and Kapoor, A. (2014). A novel approach for state of charge estimation based on adaptive switching gain sliding mode observer in electric vehicles. J. Power Sources *246*, 667–678.

Dai, H., Zhang, X., Wei, X., Sun, Z., Wang, J., and Hu, F. (2013). Cell-bms validation with a hardware-in-the-loop simulation of lithium-ion battery cells for electric vehicles. Int. J. Electr. Power Energy Syst. *52*, 174–184.

Dey, S., Ayalew, B., and Pisu, P. (2015). Nonlinear robust observers for state-of-charge estimation of lithium-ion cells based on a reduced electrochemical model. IEEE Trans. Control Syst. Technol. *23*, 1935–1942.

Di Domenico, D., Stefanopoulou, A., and Fiengo, G. (2010). Lithium-ion battery state of charge and critical surface charge estimation using an electrochemical model-based extended kalman filter. J. dyn. Syst. Meas. Control *132*, 061302.

Doyle, M., Fuller, T.F., and Newman, J. (1993). Modeling of galvanostatic charge and discharge of the lithium/polymer/insertion cell. J. Electrochem. Soc. *140*, 1526–1533.

He, H., Xiong, R., and Peng, J. (2016). Real-time estimation of battery state-of-charge with unscented kalman filter and rtos µcos-ii platform. Appl. Energy *162*, 1410–1418.

He, Y., Liu, W., and Koch, B.J. (2010). Battery algorithm verification and development using hardware-in-the-loop testing. J. Power Sources *195*, 2969–2974.

Kim, I.S. (2006). The novel state of charge estimation method for lithium battery using sliding mode observer. J. Power Sources *163*, 584–590.

Kim, N., Vijayagopal, R., Lee, D., Rousseau, A., Kwon, J., Honel, B., and Haggard, E. (2014a). Battery in the loop: battery evaluation in a systems context. In 2014 IEEE Transportation Electrification Conference and Expo (ITEC) (IEEE), pp. 1–9.

Kim, Y., Salvi, A., Siegel, J.B., Filipi, Z.S., Stefanopoulou, A.G., and Ersal, T. (2014b). Hardware-in-the-loop validation of a power management strategy for hybrid powertrains. Control Eng. Pract. *29*, 277–286.

Moura, S.J., Argomedo, F.B., Klein, R., Mirtabatabaei, A., and Krstic, M. (2017). Battery state estimation for a single particle model with electrolyte dynamics. IEEE Trans. Control Syst. Technol. *25*, 453–468.

Rahimi-Eichi, H., Ojha, U., Baronti, F., and Chow, M.Y. (2013). Battery management system: an overview of its application in the smart grid and electric vehicles. IEEE Ind. Electron. Mag. *7*, 4–16.

Santhanagopalan, S., Guo, Q., Ramadass, P., and White, R.E. (2006). Review of models for predicting the cycling performance of lithium ion batteries. J. Power Sources *156*, 620–628.

Song, H.S., Kim, T.H., Jeong, J.B., Kim, B.H., Shin, D.H., Lee, B.H., and Heo, H. (2013). Verification of battery system model for environmentally friendly vehicles using a battery hardware-in-the-loop simulation. IET Power Electron. *6*, 417–424.

Tara, E., Filizadeh, S., and Dirks, E. (2013). Battery-in-the-loop simulation of a planetary-gear-based hybrid electric vehicle. IEEE Trans. Veh. Technol. *62*, 573–581.

Wang, Q., Ping, P., Zhao, X., Chu, G., Sun, J., and Chen, C. (2012). Thermal runaway caused fire and explosion of lithium ion battery. J. Power Sources *208*, 210–224.

Zhang, W., Sun, X., Wang, L., 2017. Battery pack state of charge estimation and hardware in loop system design verification, in: 2017 9th International Conference on Intelligent Human-Machine Systems and Cybernetics (IHMSC), IEEE. pp. 331–336.

Zhang, Y., Lu, S., Yang, Y., and Guo, Q. (2018). Internet-distributed vehicle-in-the-loop simulation for hevs. IEEE Trans. Veh. Technol. *67*, 3729–3739.

Zhang, Y., Xiong, R., He, H., and Shen, W. (2016). Lithium-ion battery pack state of charge and state of energy estimation algorithms using a hardware-in-the-loop validation. IEEE Trans. Power Electron. *32*, 4421–4431.

iScience, Volume *23*

Supplemental Information

Pushing the Envelope in Battery Estimation Algorithms

Anirudh Allam, Edoardo Catenaro, and Simona Onori

Supplemental Information

Transparent Methods

Experimental Procedure

Experiments were carried out at the Stanford Energy Control Laboratory, in the Energy Resources Engineering Department, Stanford University. The equipment components, labeled in Fig. S1A, include an host computer used to program test profiles and real-time data monitoring through the MITS Pro and Data Watcher software (label 1), the Arbin LBT21024 with a programmable power supply (label 2), a battery cell positioned in a high-current cylindrical cell holder (maximum current of 200A) manufactured by Arbin (label 3), the Arbin measurement system (label 4), an embedded controller dSPACE MicroAutoBox-II (label 5), and a dSPACE Control Desk software to supervise dSPACE simulator real-time data (label 6), which provides a platform to test in real-time the design of control/estimation algorithms. The BIL architecture relies on a CAN BUS connection between battery (Arbin system) and dSPACE controller (ECU), represented in Fig. S1A.

Data communication between different equipment components is outlined in Fig. S1B and described as follows. The input current profile is configured via the MITS Pro software, which is transmitted through the TCP/IP connection to the Arbin LBT21024, before being subjected to the cell under test. The behavior of the cell in response to the current stimuli is measured by the Arbin LBT21024 in the form of voltage response. The measured current and voltage signals are sent by Arbin LBT21024 to the Arbin measurement system through the TCP/IP connection, which are then transmitetd through the CAN bus to the dSPACE MicroAutoBox-II controller. In order to access and monitor dSPACE MicroAutoBox-II real-time data for processing, data are transmitted through TCP/IP to the host computer equipped with dSPACE ControlDesk software.

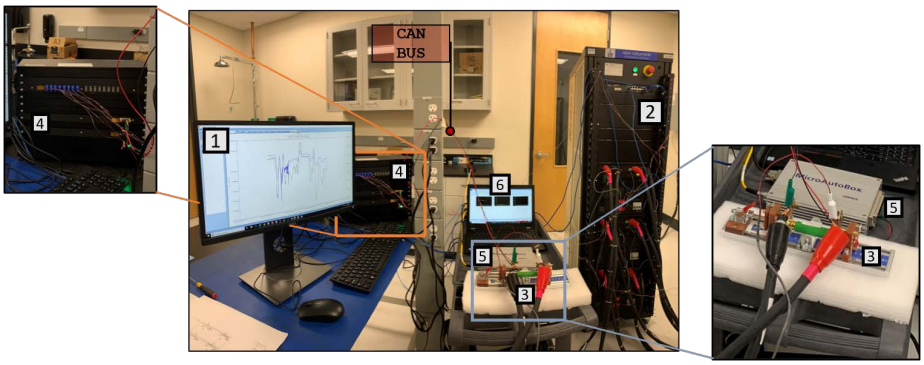

(A)

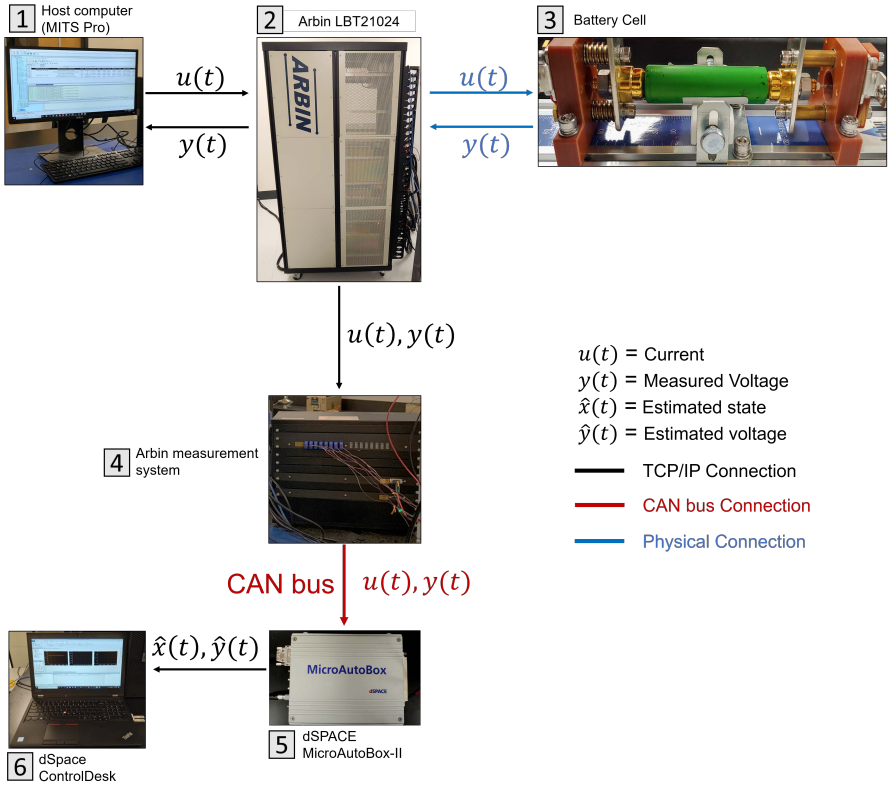

(B)

Figure S1: (A) Experimental setup at the Stanford Energy Control Laboratory. (B) Communication signals between each laboratory equipment component. Related to the physical/experimental realization of Figure 1.

Electrochemical Modeling

The conservation of mass in the solid phase governs the transport of lithium in the solid phase of each electrode ($j = [n, p]$, where n stands for negative electrode and p is for positive electrode) described by the following PDE and its respective boundary conditions

$$\begin{cases} \dfrac{\partial c_{s,j}}{\partial t} = D_{s,j}\left[\dfrac{2}{r}\dfrac{\partial c_{s,j}}{\partial r} + \dfrac{\partial^2 c_{s,j}}{\partial r^2}\right] \\ \left.\dfrac{\partial c_{s,j}}{\partial r}\right|_{r=0} = 0; \quad \left.\dfrac{\partial c_{s,j}}{\partial r}\right|_{r=R_j} = \dfrac{\pm I_{batt}}{F a_{s,j} D_{s,j} A L_j}. \end{cases} \tag{1}$$

The overpotential of each electrode is obtained from the Butler-Volmer kinetic equation that describes the rate of intercalation and de-intercalation of lithium ions as

$$\eta_j = \frac{R_g T}{0.5F} \cdot \sinh^{-1}\left(\frac{I_{batt}}{2 a_{s,j} A L_j i_{0,j}}\right) \tag{2}$$

where the exchange current density $i_{0,j} = F k_j \sqrt{c_{e,0} c_{s,j,surf} \left(c_{s,j,max} - c_{s,j,surf}\right)}$. By exploiting the relationship between capacity and power fade due to SEI layer growth at the anode, an aging-enhanced expression for the cell terminal voltage is derived as (Allam and Onori, 2020)

$$\begin{aligned} V = &\left[U_p\left(c_{s,p,surf}\right) + \eta_p\left(c_{s,p,surf}, I_{batt}\right)\right] - \\ &\left[U_n\left(c_{s,n,surf},\right) + \eta_n\left(c_{s,n,surf}, I_{batt}\right)\right] - \\ &- I_{batt}(t) R_{e,0} - I_{batt}(t) R_l - I_{batt}(t) R_{pf}(t), \end{aligned} \tag{3}$$

where U_j is the open circuit potential of the electrode which is a function of the stoichiometry ratio, θ_j that depends on the respective surface concentration as $\theta_j = c_{s,j,surf}/c_{s,j,max}$, and $R_{e,0}$ is the initial electrolyte resistance at the beginning of life expressed as (Di Domenico et al., 2010)

$$R_e = \frac{1}{2A}\left(\frac{L_n}{\kappa_n \epsilon_{e,n}^{1.5}} + \frac{2L_s}{\kappa_s \epsilon_{e,s}^{1.5}} + \frac{L_p}{\kappa_p \epsilon_{e,p}^{1.5}}\right). \tag{4}$$

For the real-time implementation of the aging-enhanced SPM, the Partial Differential Equation (PDE) describing the transport of lithium in the solid phase,

given in (1), is spatially discretized using the Finite Difference Method (FDM) into $N+1$ concentration nodes. The resulting system of Ordinary Differential Equations (ODEs) for both electrodes of the dimension $2N$ is represented using a state-space model for the ease of observer development and implementation. The state vector is considered to be $x = [x_1, x_2, x_3,]^T \in \mathbb{R}^{(2N+1)\times 1}$, $u = I_{batt}$ is the input current, and $y = V$ is the cell terminal voltage. The state variables represent lithium concentration in cathode $x_1 = [c_{s,p,1}, c_{s,p,2}, \ldots, c_{s,p,N}]^T$, anode $x_2 = [c_{s,n,1}, c_{s,n,2}, \ldots, c_{s,n,N}]^T$, and cell capacity $x_3 = Q$. It is to be noted that cell capacity is not an actual state, but augmented to the state vector to enable its estimation. The dynamics of capacity degradation are slowly varying, hence the time derivative is considered zero for practical purposes $\dot{Q} = 0$. Moreover, the surface concentration in both electrodes is given as $c_{s,j,surf} = Cc_{s,j}$, respectively, where C is the output distribution vector given as $C = [0\ 0 \ldots 1]$. Then the state space formulation of SPM is given by

$$\begin{aligned}
\dot{x}_1(t) &= A_{11}x_1(t) + B_1 u(t) \\
\dot{x}_2(t) &= \theta_1 \bar{A}_{22}x_2(t) + B_2 u(t) \\
\dot{x}_3(t) &= 0 \\
y(t) &= h_1(x_{1,N}, u) - h_2(x_{2,N}, u) - h_3(x_3)u - \\
&\quad - R_l u + (x_3 - Q_0)\theta_2 u,
\end{aligned} \tag{5}$$

where nonlinearities in the terminal voltage equation, and parameters are

$$\begin{aligned}
h_1(x_{1,N}, u) &= \left[U_p\left(c_{s,p,surf}\right) + \eta_p\left(c_{s,p,surf}, I_{batt}\right)\right], \\
h_2(x_{2,N}, u) &= \left[U_n\left(c_{s,n,surf}\right) + \eta_n\left(c_{s,n,surf}, I_{batt}\right)\right], \\
h_3(x_3) &= R_e, \\
\theta_1 &= D_{s,n}, \\
\theta_2 &= \frac{3600 M_{sei}}{2FA^2\rho_{sei}a_{s,n}^2 L_n^2 \kappa_{sei}},
\end{aligned}$$

and square matrices $A_{11}, \bar{A}_{22} \in \mathbb{R}^{N\times N}$ are the coefficients of the concentration states in (5), and column vectors $B_1, B_2 \in \mathbb{R}^{N\times 1}$ are coefficients of input current

in (5), as given below

$$A_{11} = \frac{D_{s,p}}{\Delta_r^2} \begin{bmatrix} -2 & 2 & 0 & \cdots & 0 & 0 \\ 1/2 & -2 & 3/2 & \cdots & 0 & 0 \\ \vdots & \vdots & \vdots & \ddots & \vdots & \vdots \\ 0 & 0 & 0 & \cdots & 2 & -2 \end{bmatrix} \tag{6}$$

$$B_1 = \frac{-2}{\Delta_r F a_{s,p} A L_p} \begin{bmatrix} 0 \\ 0 \\ \vdots \\ \frac{N+1}{N} \end{bmatrix}$$

$$\bar{A}_{22} = \frac{1}{\Delta_r^2} \begin{bmatrix} -2 & 2 & 0 & \cdots & 0 & 0 \\ 1/2 & -2 & 3/2 & \cdots & 0 & 0 \\ \vdots & \vdots & \vdots & \ddots & \vdots & \vdots \\ 0 & 0 & 0 & \cdots & 2 & -2 \end{bmatrix}$$

$$B_2 = \frac{2}{\Delta_r F a_{s,n} A L_n} \begin{bmatrix} 0 \\ 0 \\ \vdots \\ \frac{N+1}{N} \end{bmatrix}.$$

The procedure used to identify the model parameters, and validate it against experimental data is outlined (Allam and Onori, 2020). Further, the identified parameter values are listed in Table S1, and the rest of the geometrical and aging parameters are borrowed. (Allam and Onori, 2018; Prada et al., 2013). Further, note that the bulk SOC of the cell is limited by the cathode. Hence, the bulk SOC of the cell is computed by volume-averaging the concentration values at all discretization grid points in the cathode and normalizing it with respect to the cathode's maximum and minimum stoichiometry values, as given

Table S1: SPM Parameters. Related to Figure 2A.

Parameter	Value
L_n [m]	60.6×10^{-6}
L_p [m]	52.5×10^{-6}
A [m^2]	0.093
$c_{s,n,max}$ [mol m^{-3}]	27920
$c_{s,p,max}$ [mol m^{-3}]	45711
ϵ_n[−]	0.53
ϵ_p[−]	0.54
$D_{s,n,ref}$ [m^2 s^{-1}]	1.74×10^{-14}
$D_{s,p,ref}$ [m^2 s^{-1}]	2.98×10^{-14}
k_n[m$^{2.5}$ mol$^{-0.5}$ s^{-1}]	3.16×10^{-10}
k_p [m$^{2.5}$ mol$^{-0.5}$ s^{-1}]	5.96×10^{-10}
R_l [Ω]	0.026
L_s [m]	21×10^{-6}
ϵ_s[−]	0.58

below:

$$c_{s,p,bulk} = \frac{1}{\frac{4}{3}\pi N^3} \sum_{i=1}^{N} 4\pi i^2 c_{s,p,i}, \tag{7}$$

$$SOC = \frac{\theta_{p,0\%} - \dfrac{c_{s,p,bulk}}{c_{s,p,max}}}{\theta_{p,0\%} - \theta_{p,100\%}} \tag{8}$$

For the numerical implementation of continuous-time systems in physical embedded controllers such as the dSPACE MicroAutoBox-II, the continuous-time systems are approximated in a discretized time fashion by selecting a sampling time or time step (Δk). The discrete-time representation of the battery model is given below:

$$
\begin{aligned}
x_1\left[k+1\right] &= \left(I + A_{11}\Delta k\right) x_1\left[k\right] + B_1 u\left[k\right]\Delta k \\
x_2\left[k+1\right] &= \left(I + \theta_1 \bar{A}_{22}\Delta k\right) x_2\left[k\right] + B_2 u\left[k\right]\Delta k \\
x_3\left[k+1\right] &= x_3\left[k\right] \qquad (9) \\
y[k] &= h_1(x_{1,N}[k], u) - h_2(x_{2,N}[k], u) - \\
&\quad h_3(x_3[k])u[k] - R_l u[k] + \left(x_3[k] - Q_0\right)\theta_2 u[k], \qquad (10)
\end{aligned}
$$

where $I \in \mathbb{R}^{N\times N}$ is the identity matrix, and k is the discrete sample time.

Observer Design

The adaptive interconnected sliding mode observer for combined estimation of lithium concentration (SOC), capacity (SOH), and aging-sensitive parameters consists of two parts: *cathode observer* and an *anode observer*. The two aging-sensitive parameters that are adaptively estimated are the anode diffusion coefficient (θ_1) and SEI layer ionic conductivity (θ_2), which are moderately sensitive to the measured cell voltage (Ramadass et al., 2003; Edouard et al., 2016). The parameter θ_1 appears in the anode concentration dynamics and hence it is estimated via the anode observer. On the other hand, the parameter θ_2 appears in the system output equation and hence can be estimated via either observer, anode or cathode, as per the designer's choice. In this work, the cathode observer is used to estimate the parameter θ_2, which also aids in systematically deriving the stability proof of the adaptive interconnected observer as documented in (Allam and Onori, 2020). The discrete-time formulation of a *cathode observer* is

$$
\begin{aligned}
\hat{x}_1[k+1] =& (I + A_{11}\Delta k)\hat{x}_1[k] + \big(B_1 u[k] + \\
& G_1\left(y[k] - \hat{y}_1[k]\right) + G_{v1}\,\mathrm{sgn}\left(y[k] - \hat{y}_1[k]\right)\big)\Delta k \\
\hat{x}_{2,ol}[k+1] =& \left(I + \hat{\theta}_1[k]\bar{A}_{22}\Delta k\right)\hat{x}_2[k] + B_2 u[k]\Delta k \\
\hat{x}_3[k+1] =& x_3[k] + G_3\left(y[k] - \hat{y}_1[k]\right)u[k]\Delta k \\
\hat{y}_1[k] =& h_1\left(\hat{x}_{1,N}[k], u[k]\right) - h_2\left(\hat{x}_{2,N,ol}[k], u[k]\right) - \\
& R_l u[k] - h_3(\hat{x}_3[k])u[k] + \\
& \left(\hat{x}_3[k] - Q_0\right)\hat{\theta}_2[k]u[k],
\end{aligned} \tag{11}
$$

and *anode observer* is

$$
\begin{aligned}
\hat{x}_{1,ol}[k+1] =& \left(I + A_{11}\Delta k\right)\hat{x}_1[k] + B_1 u[k]\Delta k \\
\hat{x}_2[k+1] =& \left(I + \hat{\theta}_1[k]\bar{A}_{22}\Delta k\right)\hat{x}_2[k] + \big(B_2 u[k] + \\
& G_2\left(y[k] - \hat{y}_2[k]\right) + G_{v2}\,\mathrm{sgn}\left(y[k] - \hat{y}_2[k]\right)\big)\Delta k \\
\hat{y}_2[k] =& h_1\left(\hat{x}_{1,N,ol}[k], u[k]\right) - h_2\left(\hat{x}_{2,N}[k], u[k]\right) - \\
& R_l u[k] - h_3(\hat{x}_3[k])u[k] + \\
& \left(\hat{x}_3[k] - Q_0\right)\hat{\theta}_2[k]u[k].
\end{aligned} \tag{12}
$$

In (11) and (12), the subscript *ol* stands for open loop model state variables, $G_1 \in \mathbb{R}_-^{N\times 1}, G_2 \in \mathbb{R}_+^{N\times 1}$, $G_3 \in \mathbb{R}$ are constant linear observer gains, $G_{v1}, G_{v2} \in \mathbb{R}^{N\times 1}$ are variable structure gains, introduced to improve robustness against uncertainties, with discontinuous injection terms defined as

$$
\mathrm{sgn}\left(y - \hat{y}_i\right) = \begin{cases} 1, & \text{if } y - \hat{y}_i > 0 \\ 0, & \text{if } y - \hat{y}_i = 0 \\ -1, & \text{if } y - \hat{y}_i < 0. \end{cases} \quad i = 1, 2.
$$

The estimation error dynamics of the aforementioned adaptive interconnected sliding mode based observer is proved using Lyapunov's stability theory.(Allam and Onori, 2020)

BIL Experimental Setup

For the BIL experiments, a cylindrical lithium-ion cell is investigated, whose representation and manufacturer specifications are reported in Table S2. Further, the technical specifications of the BIL components introduced in Section are provided in Table S3.

Chemistry Composition	$LiNiMgCoO_2$/graphite
Manufacturer	Sony
Manufacturer Model	US18650VTC4
Diameter x Length [mm x mm]	18.35 x 65.2
Weight $M_{nom,cell}$ [g]	45
Nominal Voltage V_{nom} [V]	3.7
Nominal Capacity Q_{nom} [Ah]	2.1
Charging Voltage V_{charge} [V]	4.2
Charging Current I_{charge} [A]	2
Cut-off Voltage V_{cutoff} [V]	2.5
Maximum Voltage V_{max} [V]	4.2

Table S2: Manufacturer specifications for the cylindrical, fresh NMC cell used in this work. Related to Figure 2A.

The key element is establishing the BIL is the CAN bus communication between the battery testing system and the embedded controller, which is implemented both in terms of hardware and software. The CAN is a serial communication protocol used in automobiles for efficient and high speed transfer of electrical signals between multiple ECUs. The information exchange between ECUs is in the form of messages with a unique identifier (or ID) that contain the values of physical variables. In this paper, CAN messages containing the cell current and voltage information are transmitted from the Arbin battery measurement system (CAN channel 1) to the dSPACE AutoMicroBox-II (CAN

Laboratory Equipment	Manufacturer Technical Specifications	
Arbin battery test system	Manufacturer	Arbin Instruments
	Model	LBT21024
	Number of Channels	6
	Voltage Range [V]	$0-5$
	Current Ranges [A]	± 0.5, ± 5, ± 50 and ± 250
	Maximum Continuous Output Power [W]	1250
	Measurement Resolution	24-bit
	Simulation Control	Current/Power Simulation
	Auxiliaries	Temperature Measurement
	AC Power Input	3-Phase 50/60Hz 208VAC
		Input Power: 17400VA
Arbin Measurement System	Manufacturer	Amerex Instrument
	Model	LBT21024
	Voltage [V]	$90-264$
	Max. Current	220V 1.6A / 110V 3.2A
	Max Power [VA]	350
	Phase	1
dSPACE MicroAutoBox-II 1401/1513	Manufacturer	dSPACE
	Processor	IBM PPC 750GL, 900 MHz
		(incl. 1 MB level 2 cache)
	Main Memory [MB]	16
	Boot Time	1MB application, 160 ms
		3MB application, 340 ms
	CAN Interface	6 CAN channels
	Input/output Resolution	32 16-bit ch./8 16-bit ch.
	Input and output voltage range [V]	-10,+10

Table S3: Technical specifications of the Arbin battery test system, Arbin measurement system, dSPACE Scalexio simulator and dSPACE MicroAutoBox-II 1401/1513. Related to Figure 1.

channel 1).

The CAN hardware implementation via physical wiring is visualizd in Fig. S2. On the Arbin battery measurement system side, a D-Sub connector (model 171-009-113R911) is used to setup the electrical connection. The low and high voltage CAN pins of the D-Sub connector, CAN_L and CAN_H, respectively, are connected to the high and low voltage CAN pins of the dSPACE AutoMicroBox-II CAN channel 1.

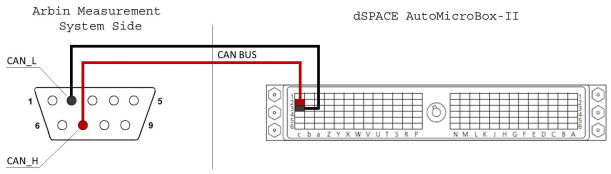

Figure S2: CAN bus connection between the Arbin battery measurement system and the dSPACE AutoMicroBox-II. The red wire (high voltage) is connected to the CAN_H pin of the D-Sub connector (Arbin battery measurement system side) and to the CAN 1 high on the dSPACE AutoMicroBox-II side. In the same way, the black wire (low voltage) is connected to the CAN_L pin and to the CAN 1 low. Related to Figure 1.

The CAN software implementation involves configuring the CAN messages, setting the baud rate, and finalizing the transmission and receiving frequency of the messages. The necessary steps are outlined below:

1. **CAN bus configuration with MITS Pro software:** This step addresses the activation of the CAN communication channel on the Arbin battery system. The MITS Pro Software, installed on the host computer labeled by 1 in Fig. S1A, is used to adjust communication settings. The current profile to be applied to the battery cell is configured in the *Schedule Files* window of MITS Pro. The current profile is composed of a rest period, wherein the cell is soaked in the desired ambient temperature of $23°C$ during a one hour rest time period (input current set to 0), and a dynamic current profile (UDDS or WLPT drive cycle). The CAN communication settings are established by opening the *CANConfig Files* window, as shown in Fig. S3A, and setting the message properties and baud rate. A new CAN configuration file, called CANconfig_Arbin_Dspace.can, is created and the sub-windows of which are described as follows:

    - *CAN Global*: the baud rate is set to 500K.
    - *Inbound CAN Signal Configuration*: Meta-variables CAN_MV_RX1 and CAN_MV_RX2, voltage and current signals, respectively, are

considered. They are transmitted through CAN message data, whose structure is defined in Fig. S3A. Note that the CAN message structure must be consistent between the transmitter and receiver system (in this paper, they correspond to the Arbin battery system and the MicroAutoBox, respectively). The *CAN Message ID* is defined as 0x100 and the *Byte Order* is set to *Little Endian*. The current and voltage signals are each 4 bytes, and hence the *Start Byte Index*, *End Byte Index*, *Start Bit Index* and *End Bit Index* are set to 0, 0, 3, 7 for the voltage message and 4, 0, 7, 7 for the current message.

- *IV Outbound CAN Message Broadcasting*: The broadcasting CAN message ID is again set to 0x100, and the desired *CAN Message Interval* is set to 100 [ms] in Fig. S3B.

Lastly, the finalized CAN configuration file CANconfig_Arbin_Dspace.can is assigned to the Arbin channel that is connected to the cell under test in the *Batch Files* window of the MITS Pro. As shown in Fig. S4, the cell under test is connected to Arbin channel 1 (*Channel index* 1), the corresponding UDDS current *Schedule* file is assigned (US18650VTC4_T23_Arbin_-Dspace_demo_UDDS.sdu), the CANconfig_Arbin_Dspace.can file is assigned to the *BMS CAN Signal Configuration File*, and the *Battery Name* is set to US18650VTC4 (which refers to battery specifications related to the ell under test reported in Table S2). The *Launch Monitor Control* window in MITS Pro launches the experiment.

2. **Real-time Interface (RTI):** The dSPACE-Simulink RTI library allows the interface between the discrete-time model-based observer implementation on Simulink with the physical input/output hardware ports of the dSPACE MicroAutoBox-II. In order to properly receive and read the CAN messages at the dSPACE AutoMicroBox-II end, which are transmitted by the Arbin system, the RTI blockset is utilized. The proposed Simulink block scheme, shown in Fig. S5, enables the embedded controller to re-

	Meta Variable Name	Nick Name	Enable	Data Log	CAN Message ID	DLC of CAN Message	Byte Order	DataType	Start Byte Index	Start Bit Index	End Byte Index	End Bit Index	Value Offset	Value Scale Factor	Unit
1	CAN_MV_RX1	Voltage	☑	Interval 500ms	0x100	8	Little Endian	Float	0	0	3	7	0	1	V
2	CAN_MV_RX2	Current	☑	Interval 500ms	0x100	8	Little Endian	Float	4	0	7	7	0	1	A

(A)

(B)

Figure S3: Tabs included in the MITS Pro software *CANConfig Files* window: (A) *Inbound CAN Signal Configuration*, describing how CAN messages are structured, and (B) *IV Outbound CAN Message Broadcasting*, which determines the broadcasting CAN message interval. Related to Figure 1.

Channel Index	Schedule	BMS CAN Signal Configuration File	Battery Name	Battery Type ID
1	US18650VTC4\US18650VTC4_T23_Arbin_Dspace_demo_UDDS.sdu	CANConfig_Arbin_Dspace.can	US18650VTC4	1

Figure S4: MITS Pro software *Batch Files* window used to assign the Arbin channel to the scheduled profile, CAN signal configuration file and battery type. Related to Figure 1.

ceive the CAN messages from the Arbin battery system that contain the real-time battery current and voltage measurements. The RTI blocks in Fig. S5 are explained below

- The *RTI Data* block is a standard block used to define the dSPACE RTI environment in Simulink.
- The *CAN Controller Setup* block is used to define the CAN controller specifications. The block settings that need to be adjusted are in the *Unit* tab: the *Mudule* is set to *CAN Type 1*, the *Controller number* to 2, the *GroupId* to *RTICAN2* and the Baudrate to 500 [kbit/s].
- the *CAN Receive Message* block determines the CAN message structure which needs to match the one previously defined for the Arbin battery system in the MITS Pro software. In the *Message* tab, the *Message identifier* is set to standard (STD), hexadecimal (hex) and 0x100, and the *Message length* is set to 8 bytes. The second tab called

Message Composition describes the process by which the model can recognize the current and voltage data within the CAN message. The composition propoerties for both signals are shown in Table. S4. In summary, using the RTI library, the properties of the CAN message to be received are set by ssigning the CAN message length to 8 bytes, corresponding to 64 bits, which is split in two parts: the first containing cell's voltage signal and the second part carrying the cell's current signal information.

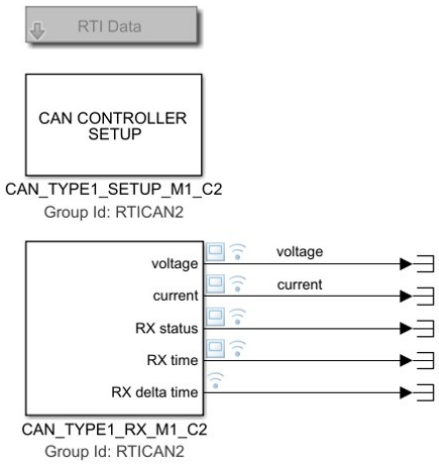

Figure S5: RTI Simulink block scheme. Related to Figure 1.

Upon configuring the RTI CAN blocks and interfacing it with the estimation algorithms, the code of the Simulink model is built and downloaded into the target platform, which is the dSPACE AutoMicroBox-II. As soon as the code is successfully flashed, the dSPACE AutoMicroBox-II light turns green. Then Arbin system measurements (current and voltage) are transmitted in real-time to the dSPACE AutoMicroBox-II through the CAN bus. Furthermore, a system description file (*.sdf), which is used in the ControlDesk software to control and visualize variables in real-time (further described in the next step).

	Current signal	Voltage signal
Signal name	current	voltage
Start bit	0	32
Signal length	32	32
Signal type	Standard	Standard
Data type	float32(IEEE)	float32(IEEE)
Byte layout	Little endian	Little endian
Factor	1	1
Factor	0	0
Physical unit	A	V

Table S4: Voltage and current signal message composition. Related to Figure 1.

3. **Real-time data monitoring on dSPACE ControlDesk:** The dSPACE ControlDesk software is used to setup a Graphical User Interface (GUI) that allows the real-time signals transmitted over the CAN bus and the estimated SOC/SOH signals to be monitored. The primary tasks associated with setting up the GUI involves

   - *Add Platform/Device*: Selecting the MABX ds1401 (corresponding to the dSPACE AutoMicroBox-II processor).
   - *Select Variable Description*: Assigning the previously generated *.sdf file corresponding to the estimation algorithm.

   The variables/parameters of the model in real-time are accessible from the *Variables Control bar* in the ControlDesk software. The GUI is populated with plotters to monitor the desired signals, such as the CAN signals (cell voltage, current, CAN communication status), and the estimated signals (SOC, SOH). When the application starts, the signals that are being monitored on the plotters are recorded, which is easily importable

to MATLAB and available for analysis.

References

Allam, A., Onori, S., 2018. An interconnected observer for concurrent estimation of bulk and surface concentration in the cathode and anode of a lithium-ion battery. IEEE Trans. on Ind. Electronics 65, 7311–7321.

Allam, A., Onori, S., 2020. Online capacity estimation for lithium-ion battery cells via an electrochemical model-based adaptive interconnected observer. IEEE Transactions on Control Systems Technology .

Di Domenico, D., Stefanopoulou, A., Fiengo, G., 2010. Lithium-ion battery state of charge and critical surface charge estimation using an electrochemical model-based extended kalman filter. Journal of dynamic systems, measurement, and control 132, 061302.

Edouard, C., Petit, M., Forgez, C., Bernard, J., Revel, R., 2016. Parameter sensitivity analysis of a simplified electrochemical and thermal model for li-ion batteries aging. J. of Power Sources , 482–494.

Prada, E., Di Domenico, D., Creff, Y., Bernard, J., Sauvant-Moynot, V., Huet, F., 2013. A simplified electrochemical and thermal aging model of lifepo4-graphite li-ion batteries: power and capacity fade simulations. Journal of The Electrochemical Society 160, A616.

Ramadass, P., Haran, B., White, R., Popov, B., 2003. Mathematical modeling of the capacity fade of li-ion cells. Journal of Power Sources 123, 230–240.